Thermally activated conductivity in gapped bilayer graphene

Maxim Trushin
Institute for Theoretical Physics, University of Regensburg, D-93040 Regensburg, Germany and Physics Department, University of Texas, 1 University Station C1600, Austin, 78712 Texas, USA
(Dated: December 20, 2011)

This is a theoretical study of electron transport in gated bilayer graphene — a novel semiconducting material with a tunable band gap. It is shown that the quantum mechanical superposition between conduction and valence band states enhances the subgap conductivity and facilitates the thermally activated transport. The mechanism proposed can also lead to the non-monotonic conductivity *vs.* temperature dependence at a band gap size of the order of 10 meV. The effect can be observed in gapped bilayer graphene sandwiched in boron nitride where the electron-hole puddles and flexural phonons are strongly suppressed.

I. INTRODUCTION

Graphene[1] is often considered[2] as a most promising material for future semiconductor industry. Indeed, it demonstrates high carrier mobility even at room temperature[3] and is suitable for mass production thanks to the chemical vapor deposition technique developed recently.[4,5] However, pristine graphene[3] does not have a band gap which is a crucial ingredient for the field effect transistor functionality. It is possible to open the gap in *bilayer* graphene by applying an external electric field perpendicular to the sample, see Fig. 1. The effect was predicted by McCann[6] and experimentally proven in Ref.[7]. Note that it is also possible to open a gap between hole and conduction bands in bilayer graphene by means of an appropriate chemical doping.[8]

In order to control the band gap and carrier density independently the double-gated graphene devices have been utilized[9–12]. The most striking feature observed is that the band gap obtained by infrared spectroscopy[13,14] turns out to be much too large to fit the thermally activated conductivity measurements. There are a few attempts to resolve this discrepancy. An earlier model[15] suggests the formation of midgap states in which charge carriers are localized. The band edge moves locally further into the gap and a hopping mechanism dominates the conduction.[9,10] The most recent approach[16] employs fluctuations of the charged impurity potential separating the electron and hole puddles. Indeed, the first experimental observations[9–11] of the insulating behavior in gapped bilayer graphene have been made in the devices with graphene flakes placed directly on the SiO_2 substrate. The substrate impurities are known to cause sizable potential fluctuations which lead to the formation of electron-hole puddles at low carrier densities.[17] If the substrate potential fluctuations are strong enough then the small effective band gap is expected to be due to the percolation through the charge inhomogeneities overwhelming the real spectral gap. The relevance of this mechanism to the subgap conductivity is unquestionable as long as graphene is placed on the SiO_2 substrate.[16] In recent experiments[12] carried out on *suspended* double-gated bilayer graphene the electron-hole puddles are expected to be suppressed; nevertheless, the activation energy deduced from the transport measurements is still smaller than the band gap size. An alternative model[18] suggests that the edge transport plays an important role in these measurements.[12] The phenomenon originates from non-trivial topological properties of the electronic band structure in graphene which are similar to those in spin-orbit induced topological insulators.[19]

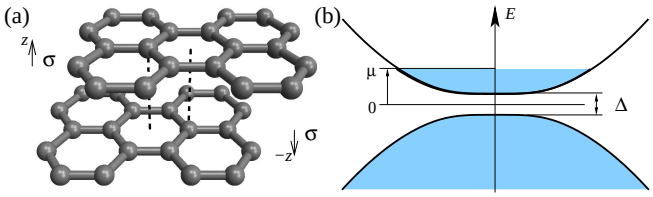

FIG. 1: Panel (a) shows bilayer graphene's crystal structure and *which-layer* pseudospin orientation. Panel (b) shows the lowest two bands and band gap size Δ. The chemical potential μ is counted from the middle of the band gap.

A question addressed in this paper is whether there is another mechanism responsible for the substantial subgap conductivity which can manifest itself in gapped bilayer graphene sandwiched in boron nitride.[20,21] Such graphene samples are practically insusceptible to the environment making the substrate much less important. Moreover, the electron-hole puddles can be completely screened out in double-layer systems similar to those recently reported in.[22] The edge transport, if any, can be precluded in Corbino geometry which has been already utilized in recent experiments carried out on double-gated bilayer graphene.[23] Using the electron-hole coherence concept we predict that the subgap conductivity contribution does not vanish completely even though all abovementioned mechanisms are excluded, see Figs. 2,3. The signature of the mechanism in question is the non-monotonic conductivity *vs.* temperature dependence at a band gap size of a few tens of meV, see Figs. 4,5. This non-monotonic dependence could not be explained within conventional model[9,10,15] where disorder renormalizes the band gap to a smaller value just by locally raising or lowering the band edges.

II. CONCEPT

We show that the difference between effective (transport) and actual (spectral) gaps is an intrinsic property of gapped bilayer graphene following from the minimal two-band effective Hamiltonian already employed in Ref.[9]. The Hamiltonian can be written as $H_0 = \vec{h}_k \cdot \vec{\sigma}$, where

$$\vec{h}_k = \frac{\hbar^2 k^2}{2m}\left(\hat{x}\cos 2\varphi + \hat{y}\sin 2\varphi\right) + \hat{z}U, \qquad (1)$$

and $\vec{\sigma}$ are Pauli matrices representing the *pseudospin*[24] degree of freedom for carriers in bilayer graphene which originates from its peculiar crystal lattice shown in Fig. 1(a) with the σ_z-pseudospin projection referring to the layer index. Here, $m \simeq 0.05m_0$ is the effective mass, m_0 is the bare electron mass, $\mathbf{k}$ is the two-component particle momentum, $\tan\varphi = k_y/k_x$, and $\Delta = 2U$ is the band gap. The eigenvalues of H_0 are $E_{\kappa\mathbf{k}} = \kappa\sqrt{\left(\frac{\hbar^2k^2}{2m}\right)^2 + U^2}$ with $\kappa = \pm$ being the band index, and the eigenstates are $\psi_{\kappa\mathbf{k}}(\mathbf{r}) = \mathrm{e}^{i\mathbf{kr}}|\chi_{\kappa k}\rangle$ with the spinors $|\chi_{+k}\rangle = (\cos\frac{\vartheta_k}{2}, \sin\frac{\vartheta_k}{2}\mathrm{e}^{2i\varphi})^T$, $|\chi_{-k}\rangle = (\sin\frac{\vartheta_k}{2}, -\cos\frac{\vartheta_k}{2}\mathrm{e}^{2i\varphi})^T$, where $\cos\vartheta_k = U/\sqrt{\left(\frac{\hbar^2k^2}{2m}\right)^2 + U^2}$. The bands $E_{\kappa\mathbf{k}}$ are shown in Fig. 1(b).

Our analysis involves the vector $\vec{\sigma}$ which always has opposite orientations in conduction and valence band eigenstates[24] for a given momentum $\mathbf{k}$ and, therefore, can be used as a band marker. If not being in the eigenstate $|\chi_{\kappa k}\rangle$, the pseudospin $\vec{\sigma}$ precesses in a way similar to the real spin precession in electron gases with spin-orbit coupling. From the quantum mechanical point of view, the pseudospin precession corresponds to the superposition of two eigenstates with the opposite pseudospin orientations. Since the pseudospin is entangled with the band index, the precession leads to the creation of a quantum mechanical superposition between conduction and valence band eigenstates. Note that such a superposition has nothing to do with the electron-hole pairs. The latter are entirely classical objects whereas the former is of quantum mechanical nature. The electron-hole pairs occur in both graphene and conventional semiconductor material as soon as the temperature reaches the level high enough to excite the valence electrons across the band gap. In contrast, due to the pseudospin precession, the carriers in graphene can *simultaneously* be in the valence and conduction bands while moving between two subsequent collisions with the scatterers. Each scattering event can be seen as a classical "measurement" which changes the carrier's wave function to either conduction or valence band eigenstate making a contribution to the total conduction even at zero temperature. At the same time the direction of the particle's motion is changed, and since the momentum and pseudospin are entangled, the particle's pseudospin gets out of its eigenstate immediately after the scattering event and starts precessing again. In that way the superposition states can facilitate the conductivity making the effective band gap smaller than the actual one, see Figs. 2–3. This phenomenon, as many other effects related to the quantum mechanical coherence, is sensitive to temperature. In some cases one can observe the competition between the temperature-dependent pseudospin decoherence and thermal activation processes which results in the non-monotonic conductivity *vs.* temperature dependence, see Figs. 3–4.

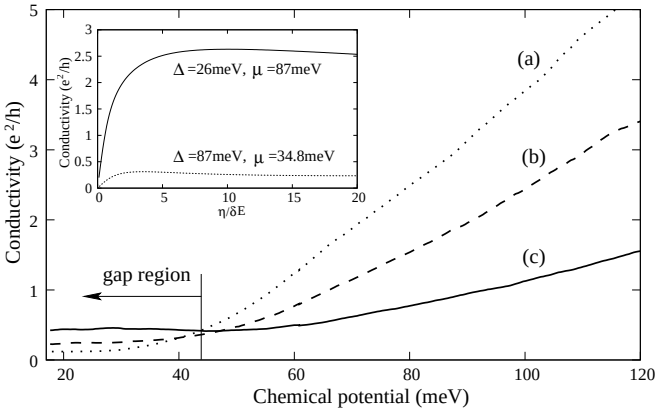

FIG. 2: Zero-temperature conductivity (for given spin and valley) of gapped bilayer graphene (band gap size $\Delta = 87\,\mathrm{meV}$) in presence of the δ-correlated disorder with the strength $u_0 = 2.74 \cdot 10^{-14}\,\mathrm{eVcm}^2$. The concentration of scatterers $n_s = N_s/L^2$ (with $L = 1.8 \times 10^{-5}\,\mathrm{cm}$ being the sample size) is different for each curve: (a) $0.54 \cdot 10^{12}\,\mathrm{cm}^{-2}$, (b) $0.81 \cdot 10^{12}\,\mathrm{cm}^{-2}$, (c) $1.62 \cdot 10^{12}\,\mathrm{cm}^{-2}$. The coupling η is chosen to be equal to $10\delta E$, where $\delta E = 2\pi\hbar^2/L^2m$. The inset shows that the dependence of both metallic and subband conductivities on η is relatively weak in this case.

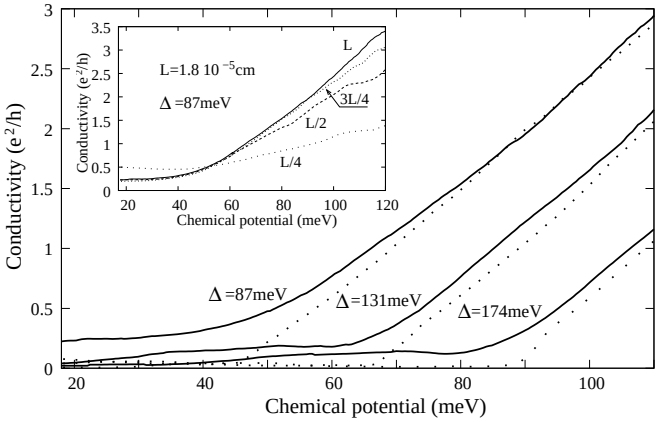

FIG. 3: Zero-temperature conductivities for gapped bilayer graphene (solid lines) and conventional intrinsic semiconductor (dotted lines) described by Eqs. (1) and (3) respectively. Note that the latter conductivity drops down to zero as soon as the Fermi energy level reaches the bottom of the conduction band. Disorder parameters are the same as in Fig. 2 for curve (b). The inset shows how the conductivity curve changes under scaling. The disorder concentration n_s is chosen to be the same for all L's considered. One can see that the conductivity gets less sensitive to scaling for larger L's considered in this work.

III. METHODS

To evaluate the *dc* conductivity σ we follow the procedure described in[25,26] and start from the finite-size Kubo formula

$$\sigma = -\frac{i\hbar e^2}{L^2}\sum_{n,n'}\frac{f^0_{E_n}-f^0_{E_{n'}}}{E_n-E_{n'}}\frac{\langle n|v_x|n'\rangle\langle n'|v_x|n\rangle}{E_n-E_{n'}+i\eta}, \qquad (2)$$

where L^2 is the finite-size system area, η is the coupling to source and drain reservoirs, $\mathbf{v}$ is the velocity operator, $f^0_{E_n}$ is the Fermi-Dirac distribution function, and $|n\rangle$ denotes an exact eigenstate of the numerically solved Schrödinger equation for a finite-size disordered system with periodic boundary conditions: $(H_0+V)\psi_n = E_n\psi_n$, where $V(\mathbf{r}) = u_0\sum_i^{N_s}\delta(\mathbf{r}-\mathbf{R}_i)$ for the short-range disorder model we consider. The scattering locations $\mathbf{R}_i$ and potential signs of u_0 are random. The Schrödinger equation has been solved using a large momentum-space cutoff $k^* \approx 7\cdot 10^6\,\mathrm{cm}^{-1}$ which corresponds to the energy scale at which the split-off bands of bilayer graphene become relevant and our two-band model no-longer applies.

The pseudospin precession (the effect in which we are mainly interested here) always occurs in graphene whichever disorder potential is assumed. The model considered here should be seen as a generic one where delta-correlated scattering potential is chosen just for the sake of simplicity even though the short range disorder mixes states in different valleys. The intervalley scattering appears to be irrelevant to any other type of disorder (charged impurities, ripples) and is therefore neglected here. Note that the Thomas–Fermi theory has been recently employed[16] to calculate the electronic structure in the presence of the disorder potential due to charge impurities in gapped bilayer graphene. The theory is quasiclassical and does not include the quantum mechanical superposition considered here. Most important is that the amplitude of the screened disorder potential fluctuations must be of the order of the gap size Δ in order to explain the difference between the spectral band gap and the experimentally extracted transport gap. Here, quite an opposite situation is considered: The scatterer strength u_0 and concentration $n_s = N_s/L^2$ are chosen to be small enough ($u_0 n_s < \Delta$) to preclude the percolative regime[16] and substantial band gap renormalization.[15] Such careful choice of disorder parameters makes it possible to observe the pseudospin coherence effects.

The Kubo conductivity (2) vanishes at $\eta \to 0$ as well as at $\eta \to \infty$. As one can see in Fig. 2(inset), there is an intermediate region near $(\eta m L^2)/(2\pi\hbar^2) = 10$ where the conductivity is not too sensitive to η. It is natural to work in this region to estimate the conductivity at a given system size L. The length L is chosen to be so large that the conductivity curves don't change too much with further increasing of L. Fig. 3(inset) shows the conductivity curves for different sample sizes starting from $\frac{1}{4}L = 0.45\times 10^{-5}\,\mathrm{cm}$ with $0.45\times 10^{-5}\,\mathrm{cm}$ step. One can see that the difference in the conductivity behavior for the lengths $\frac{3}{4}L = 1.35\times 10^{-5}\,\mathrm{cm}$ and $L = 1.8\times 10^{-5}\,\mathrm{cm}$ becomes rather small, thus, the latter is chosen to be the typical sample size which allows the scaling with L. The typical scatterer number N_s is a few hundreds for this L. The momentum cut-off k^* and L fix the Hamiltonian matrix dimension at 3362×3362.

The zero-temperature conductivity curves depicted in Figs. 2,3 are smoothed by averaging over an energy interval containing 10–100 levels, over boundary conditions, and over several disorder potential realizations.[26] The finite-temperature conductivity demonstrates much weaker fluctuations, thus, the results shown in Figs. 4,5 are averaged just over a few disorder realizations.

IV. RESULTS

As one can see from Fig. 2, the conductivity does not vanish even though the chemical potential μ gets below the bottom of the conduction band and the temperature is zero. Moreover, the subgap conductivity *increases* with disorder (cf. Ref.[27]). This peculiar behavior can be understood in terms of the disorder-dependent quasiparticle life-time τ and pseudospin decoherence time $\tau_{\mathrm{dc}} = \hbar/2E_k$ with E_k being the characteristic particle energy. The latter equals to either μ or $\Delta/2$ whichever is larger. The pseudospin precession in disordered graphene leads to the randomization of any initial pseudospin state making the electron transport pseudospin-incoherent.[26] However, if the disorder gets stronger, then the pseudospin has less time to change its orientation between two subsequent scattering events and the transport becomes more pseudospin-coherent. As consequence, the subgap pseudospin-coherent conductivity contribution increases with disorder — the effect we actually observe in Fig. 2. The upper limit for quasiparticle life-time τ (which is the same as the momentum relaxation time in presence of the short-range disorder potential) can be estimated using the Fermi golden-rule at $\mu \gg U$ as $\tau \simeq 3\cdot 10^{-14}\,\mathrm{s}$ corresponding to the mobility $10^3\,\mathrm{cm}^2/\mathrm{Vs}$ for curve (b).

Looking at the plots in Fig. 2 one might still think that it is the impurity density of states, rather than the pseudospin precession, that is responsible for finite subgap conductivity. In order to clarify this issue let us compare the pseudospin-momentum coupled model (1) with the decoupled one in which $H_0' = \vec{h}_k'\cdot\vec{\sigma}$, where

$$\vec{h}_k' = \hat{x}\frac{\hbar^2k^2}{2m} + \hat{z}U. \qquad (3)$$

The two models have the same energy spectrum, but the the eigenstate spinors do not depend on the direction of particle's motion here and read $|\chi'_{+k}\rangle = (\cos\frac{\vartheta_k}{2}, \sin\frac{\vartheta_k}{2})^T$, $|\chi'_{-k}\rangle = (\sin\frac{\vartheta_k}{2}, -\cos\frac{\vartheta_k}{2})^T$. Either conduction or valence band eigenstate once created can propagate through the disordered sample without changing its pseudospin orientation even though the direction of motion is altered after each scattering event. The interband superposition states do not occur here and the

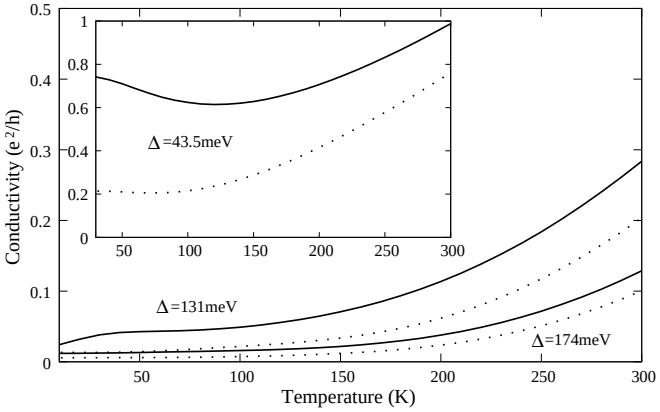

FIG. 4: Thermally activated conductivity at different band gap size Δ for gapped bilayer graphene (solid lines) and decoupled band intrinsic semiconductor (dotted lines) described by Eqs. (1) and (3) respectively. The chemical potential is zero, i. e. it is placed exactly in the middle of the gap. The subgap conductivity increases slower with the temperature within the decoupled band model. The inset shows the competition between the temperature-dependent pseudospin decoherence and thermal activation processes resulting in the non-monotonic temperature dependence of graphene's conductivity at smaller band gap. Besides the band gap size shown in the plot, all other parameters are the same as in Fig. 2 for curve (b).

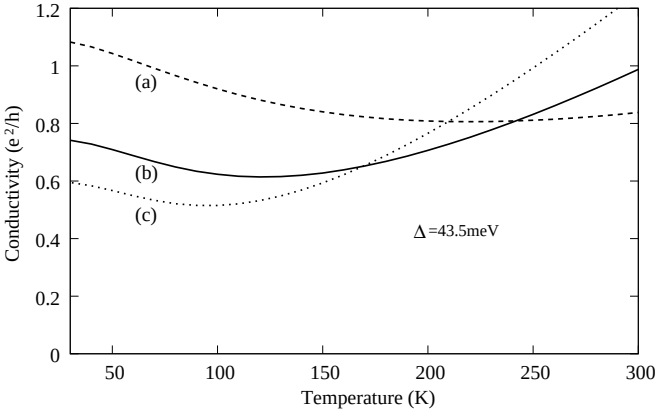

FIG. 5: This figure demonstrates the non-monotonic behavior of thermally activated conductivity for bilayer graphene at the intermediate band gap size $\Delta = 43.5\,\mathrm{meV}$ for different disorder concentrations n_s. The chemical potential is zero, and disorder parameters for each curve are the same as in Fig. 2.

conductivity vanishes as soon as the chemical potential reaches the bottom of the conduction band, see dotted lines in Fig. 3. In contrast, gapped bilayer graphene demonstrates a substantial subgap conductivity at the same parameters. Thus, to observe this effect (i) the pseudospin must be coupled with the particle momentum to create the interband superposition states in disordered samples and (ii) the system must be pseudospin-coherent, i. e. τ/τ_{dc} must be smaller than one. Note that $\tau_{\mathrm{dc}} = \hbar/2\mu$ (for $\mu > \Delta/2$) decreases with increasing μ making the two conductivities in Fig. 3 indistinguishable at higher carrier concentrations.

The difference between bilayer graphene described by Eq. (1) and its rival with decoupled bands (3) at best can be seen in the thermally activated conductivity. The calculations can also be considered as a simulation of the charge transport in a field effect transistor turned to the "off" state when the chemical potential is placed exactly in the middle of the band gap hampering both electron and hole transport at low temperatures. As it is seen in Fig. 4, the pseudospin-coupled carriers can be excited easier than the decoupled ones. The difference between conductivities in these two cases becomes essential at room temperatures. Note that if $T \ll \Delta$, then the *pseudospin-incoherent* conductivity can be well described by the classical formula $\frac{\tau T}{\hbar}\exp(-\frac{\Delta}{2T})$ indicating that the thermally activated conductivity always increases with temperature. In contrast, the subgap *pseudospin-coherent* conductivity decreases as soon as T becomes comparable with $\Delta/2$ substituting the latter in the expression for τ_{dc} and breaking down the pseudospin-coherence. The competition between these two mechanisms can result in the non-monotonic temperature dependence of graphene's conductivity, see Fig. 4(inset). Note that if $T \gg \Delta$, then both conductivity curves coincide. (This regime is not shown in figure.)

The non-monotonic conductivity behavior is robust under moderate change of the disorder strength, see Fig. 5. However, as it is mentioned in Section III, the disorder strength $n_s u_0$ must always be smaller than the band gap size in order preclude the influence of midgap states. The bilayer samples must therefore be relatively clean to observe the non-monotonic conductivity behavior predicted here. The necessary quality can probably be achieved in graphene on boron nitride.[21] It is also important that the phonons, which are not considered here at all, might spoil the effect. The phonon resistivity contribution in bilayer graphene is dominated by flexural phonons and rapidly increases with temperature.[28] The flexural phonons can be again suppressed in graphene sandwiched between boron nitride layers.[20–22]

V. CONCLUSION

To conclude, there is a fundamental obstacle which limits the functionality of the field effect transistor based on gapped bilayer graphene. The physical mechanism responsible for that is intimately linked to the pseudospin precession which can be seen as an instantaneous generation of conduction-valence band superposition states. Such states lead to higher "leakage" current in the "off" state and therefore limit the possible on/off ratio by lower values as compared to those in conventional semiconductor devices with the same mobility and band gap size. In contrast to the "leakage" mech-

anisms considered before,[15,16,18] the superposition state effect described here is unavoidable unless the very crystal lattice is broken. The non-monotonic conductivity *vs.* temperature dependence predicted here can be seen as a signature of the pseudospin precession responsible for the difference between the transport and spectral gaps. The effect can probably be observed in doubly gated bilayer graphene sandwiched between boron nitride layers where the charge inhomogeneity and flexural phonon conductivity contributions are substantially reduced.

Acknowledgments

I would like to thank Prof. Allan MacDonald for his hospitality during my stay at the University of Texas at Austin, where a part of this work has been done, and DFG for financial support through the project TR 1019/1-1.

[1] K. S. Novoselov, A. K. Geim, S. V. Morozov, D. Jiang, M. I. Katsnelson, I. V. Grigorieva, S. V. Dubonos, and A. A. Firsov, Nature **438**, 197 (2005).
[2] F. Schwierz, Nature Nanotech. **5**, 487 (2010).
[3] A. K. Geim and K. S. Novoselov, Nat. Mat. **6**, 183 (2007).
[4] I. Jeon, H. Yang, S.-H. Lee, J. Heo, D. H. Seo, J. Shin, U.-I. Chung, Z. G. Kim, H.-J. Chung, and S. Seo, ACS Nano **5**, 1915 (2011).
[5] M. P. Levendorf, C. S. Ruiz-Vargas, S. Garg, and J. Park, Nano Letters **9**, 4479 (2009).
[6] E. McCann, Phys. Rev. B **74**, 161403 (2006).
[7] E. V. Castro, K. S. Novoselov, S. V. Morozov, N. M. R. Peres, J. M. B. Lopes dos Santos, J. Nilsson, F. Guinea, A. K. Geim, and A. H. Castro Neto, Phys. Rev. Lett. **99**, 216802 (2007).
[8] T. Ohta, A. Bostwick, T. Seyller, K. Horn, and E. Rotenberg, **313**, 951 (2006).
[9] J. B. Oostinga, H. B. Heersche, X. Liu, A. F. Morpurgo, and L. M. K. Vandersypen, Nature Materials **7**, 151 (2008).
[10] T. Taychatanapat and P. Jarillo-Herrero, Phys. Rev. Lett. **105**, 166601 (2010).
[11] K. Zou and J. Zhu, Phys. Rev. B **82**, 081407 (2010).
[12] R. T. Weitz, M. T. Allen, B. E. Feldman, J. Martin, and A. Yacoby, Science **330**, 812 (2010).
[13] Y. Zhang, T.-T. Tang, C. Girit, Z. Hao, M. C. Martin, A. Zettl, M. F. Crommie, Y. R. Shen, and F. Wang, Nature **459**, 820 (2009).
[14] K. F. Mak, C. H. Lui, J. Shan, and T. F. Heinz, Phys. Rev. Lett. **102**, 256405 (2009).
[15] J. Nilsson and A. H. Castro Neto, Phys. Rev. Lett. **98**, 126801 (2007).
[16] E. Rossi and S. Das Sarma, Phys. Rev. Lett. **107**, 155502 (2011).
[17] J. Martin, N. Akerman, G. Ulbricht, T. Lohmann, J. H. Smet, K. von Klitzing, and A. Yacoby, Nature Physics **4**, 144 (2008).
[18] J. Li, I. Martin, M. Buttiker, and A. F. Morpurgo, Nature Phys. **7**, 38 (2011).
[19] M. Z. Hasan and C. L. Kane, Rev. Mod. Phys. **82**, 3045 (2010).
[20] A. S. Mayorov, R. V. Gorbachev, S. V. Morozov, L. Britnell, R. Jalil, L. A. Ponomarenko, P. Blake, K. S. Novoselov, K. Watanabe, T. Taniguchi, et al., Nano Letters **11**, 2396 (2011).
[21] C. R. Dean, A. F. Young, I. Meric, C. Lee, L. Wang, S. Sorgenfrei, K. Watanabe, T. Taniguchi, P. Kim, K. L. Shepard, et al., Nature Nanotech. **5**, 722 (2010).
[22] L. A. Ponomarenko, A. A. Zhukov, R. Jalil, S. V. Morozov, K. S. Novoselov, V.V. Cheianov, V.I. Fal'ko, K. Watanabe, T. Taniguchi, A. K. Geim, R. V. Gorbachev, arXiv:1107.0115.
[23] J. Yan and M. S. Fuhrer, Nano Letters **10**, 4521 (2010).
[24] M. I. Katsnelson, K. S. Novoselov, and A. K. Geim, Nature Physics **2**, 620 (2006).
[25] K. Nomura and A. H. MacDonald, Phys. Rev. Lett. **98**, 076602 (2007).
[26] M. Trushin, J. Kailasvuori, J. Schliemann, and A. H. MacDonald, Phys. Rev. B **82**, 155308 (2010).
[27] J. H. Bardarson, J. Tworzydło, P. W. Brouwer, and C. W. J. Beenakker, Phys. Rev. Lett. **99**, 106801 (2007).
[28] H. Ochoa, E. V. Castro, M. I. Katsnelson, and F. Guinea, Phys. Rev. B **83**, 235416 (2011).